Increased vulnerability of Purkinje cells in the posterior cerebellum of SCA1 mice is associated with molecular and cellular alterations related to disease pathology

Abbreviated title: Intracerebellar differences in SCA1

Katherine Hamel[1], Carrie Sheeler[1], Juao-Guilherme Rosa[1,4], Stephen Gilliat[1], Ying Zhang[1,2,3], Marija Cvetanovic[1,2*]

1. Department of Neuroscience, University of Minnesota
2. Institute for Translational Neuroscience, University of Minnesota 2101 6th Street SE, Minneapolis, MN 55455
3. Minnesota Supercomputing Institute, University of Minnesota
4. Boston University

*Corresponding Author:

Katherine Hamel, Department of Neuroscience, University of Minnesota

2101 6th Street SE, Minneapolis, MN 55455

E-mail: mcvetano@umn.edu

Tel. 612-626-4918

Abstract (112 words)

Spinocerebellar Ataxia type 1 (SCA1) is a dominantly inherited neurodegenerative disease caused by abnormal expansion of the polyglutamine (polyQ) repeats in the ATAXIN1 (ATXN1) protein. Patients with SCA1 suffer from progressive motor and cognitive impairments, without any disease modifying treatments available. Although mutant ATXN1 is expressed throughout the brain, the cerebellum undergoes the most severe degeneration. It remains unclear why the cerebellum is particularly vulnerable in SCA1.

A majority of previous studies using mouse models of SCA1 have investigated pathological changes in the cerebellar cortex by examining a singular region in the cerebellar cortex, the vermal primary fissure (lobules V and VI). Gene expression changes have mostly been examined using the bulk cerebellum. However, recent studies in patients indicate that SCA1 pathogenesis is not uniform across cerebellum, and in fact demonstrate that the posterior vermis and hemispheres exhibit worse pathology. Pathological and molecular alterations in the posterior cerebellum and hemispheres remain mostly unknown in mouse models of SCA1. This study addresses these questions using *Atxn1*$^{154Q/2Q}$ line, a knock-in SCA1 mouse model in which mutant ATXN1 is widely expressed. We found more pronounced pathology of Purkinje cells and reactive gliosis in the posterior vermis of *Atxn1*$^{154Q/2Q}$ mice at mid -disease stages, similar to what has been described in SCA1 patients. Comparison of the gene expression changes demonstrates that several cerebellar cell types, including Purkinje cells, and Bergmann glia, are more affected in the posterior vermis, and hemispheres. Pathway analysis identified discrete, region specific SCA1 pathogenesis pathways as well as commonly enriched biological pathways.

Introduction

Neurodegenerative diseases are pathologically defined by progressive degeneration and cell death within discrete regions of the brain [1][2]. For instance, in Huntington's disease (HD), mutant Huntingtin (HTT) is widely expressed yet pathology is most severe in the medium spiny neurons in the striatum. In SCA1, cerebellar Purkinje cells are most vulnerable despite wide expression of mutant ATXN1 in the brain. Thereby, perhaps the key unanswered question in neurodegeneration is what causes this selective vulnerability of brain regions and specific neural populations. An initial

step to answer this question of region-specific susceptibility is to investigate whether the pattern is reproduced in mouse models of disease followed by the examination of underlying molecular differences across unaffected and affected brain regions. Large-scale transcriptomics, such as RNAsequencing, both bulk and single-cell or single-nuclei demonstrated large regional molecular differences in neurons and glia across brain regions, complicating the identification of genes and pathways that may underlie regional susceptibility in disease. For example, studies using SCA1 mouse models compared the expression differences between the cerebellum and inferior olive and found there are distinct enriched biological pathways in each region [3][4]. While these studies highlight the benefits of examining alterations on a region-specific basis, it is not easy to distinguish which of these regional pathological differences are reflection of the physiological differences across regions and which reflect disease pathogenesis.

We propose that to further understand the mechanisms that underlie vulnerability or protection from disease progression, sub region-specific exploration of vulnerable cell populations may allow for better understanding the development, progression, and possible treatment of neurodegenerative diseases.

Spinocerebellar ataxia type-1 (SCA1) is a rare neurodegenerative disorder caused by CAG repeat expansions in the gene *Ataxin-1* (*ATXN1)*[5]. Repeat expansions of about 39 or more repeats result in expression of a toxic polyglutamine (polyQ) ATXN1 protein [6]. Although ATXN1 is expressed throughout the brain, SCA1 is characterized by progressive degeneration that is most severe in the cerebellar Purkinje cells (PCs), and manifests behaviorally as deficits in motor coordination (i.e. ataxia), cognitive and mood deficits, difficulties in swallowing and premature lethality [7][8][9][10]. While *Atxn1*-targeting antisense oligonucleotides (ASO) show promise in pre-clinical trials [11], there are currently no disease-modifying treatments available for SCA1 [12].

As mentioned above, mutant ATXN1 is expressed throughout the brain, yet cerebellum is severely affected. MRI studies showed a severe atrophy of the cerebellum and brain stem, while post- mortem

brain investigations reveal pronounced pathology in the cerebellum, including cortex and white mater, deep cerebellar nuclei and its three peduncles in patients with SCA1 [13][14].

The cerebellum is implicated in many functions, including motor and cognitive control, social cognition, reward and affect [15][16]. Anatomically cerebellum is divided into two main regions, the evolutionary-older midline vermis and the lateral hemispheres, with hemispheres significantly expanded in humans. The vermis is further divided by primary fissure into the anterior region, comprised of lobules I to V, and the posterior region, comprised of lobules VI to IX in vermis [17]. While the cerebellar cortex has remarkably uniform anatomy and circuitry though out each of the lobules across the vermis and hemispheres, a wide range of studies utilizing functional imaging, resting state connectivity, anatomical tract tracing, clinical studies of cerebellar injuries, single cell sequencing, electrophysiology, and functional connectivity indicate functional heterogeneity of the cerebellum. This heterogeneity occurs both in terms of function and connectivity with other brain regions[18][19][20][21][22][23]. For instance the primary somato-motor region of the cerebellum is located in the anterior vermis of the cerebellum and adjacent part of lobule VI, while cognitive regions of cerebellum are located in the posterior cerebellar vermis, including lobules VI, VII, and IX and hemispheres (Crus I and II)[16].

In addition to this physiological heterogeneity of the cerebellum, specific patterns of cerebellar degeneration were also identified as patients with SCA1 showed the greatest decline in hemispheres followed by lobules XI and VIII when compared with their respective age-matched and gender-matched control groups [24]. Moreover, recent longitudinal MRI study indicated significant cortical thinning in the posterior and hemisphere cerebellar lobules including lobules crus I–II, VIIB, VIIIA–B, IX, and X, while more anterior lobules were not significantly different from controls [25].
It is unclear what causes increased vulnerability of cerebellar cortex of hemispheres and posterior vermis compared to relative sparing of anterior vermis in SCA1 patients.

Mouse models have been very useful in understanding of the underlying mechanisms of SCA1 pathogenesis in cerebellum [26][27][28][29]. However, most of the pathological studies have been

focused on the primary fissure and lobules V and VI and bulk RNA expression or protein analysis [30][31][32]. Here we used *Atxn1*$^{154Q/2Q}$ SCA1 knock in mice that express mutant protein under endogenous promoter and as such have physiological levels and spatial pattern of mutant ATXN1 expression [28] to examine intracerebellar regional differences in pathology and underlying molecular causes. We found increased vulnerability of the posterior lobules in terms of PC and glial pathology, including increased dendritic atrophy and loss of synapses as well as increased reactive gliosis. These results indicate that increased vulnerability of posterior vermis seen in SCA1 patients is present in *Atxn1*$^{154Q/2Q}$ mice. Using a newly developed quick method for cerebellar dissection, we performed RNAsequencing of anterior and posterior cerebellar vermis and cerebellar hemispheres in *Atxn1*$^{154Q/2Q}$ mice and wild-type littermates. Gene expression and pathway analysis identified important neuronal and glial genes and pathways that are altered in region specific manner. The differences across these regions could point to pathways that lead to tissue vulnerability or protection from disease progression.

Materials and Methods

Mice

The creation of the *Atxn1*$^{154Q/2Q}$ mice was previously described [28]. As CAG repeats are unstable in mice we periodically sequence CAG region to evaluate number of repeats. At the time of experiments the average number of CAG repeats in our colony was 166. Experimental groups were balanced with an equal number of male and female *Atxn1*$^{154Q/2Q}$ and wild-type (WT) mice. In all experiments, investigators were blinded to the genotype.

Animal experimentation was approved by Institutional Animal Care and Use Committee (IACUC) of University of Minnesota and was conducted in accordance with the National Institutes of Health's (NIH) Principles of Laboratory Animal Care (86–23, revised 1985), and the American Physiological Society's Guiding Principles in the Use of Animals [33].

Dissection

Cerebellar anterior and posterior cortex of vermis and hemispheres were dissected as previously described [34]. Briefly, brains were placed into the brain matrix with dorsal side up, and one razor blade was placed along the sagittal midline, making sure that the blade pushes all the way to the bottom of the matrix. Additional seven razor blades were consequently positioned with 1 mm apart from each other (three on each side of the brain). In total there will be six sagittal brain sections with four most lateral sections containing hemispheres where we separated DCN from the cortex. Midline two vermal sections were cut along primary fissure to separate separating the anterior lobes from the posterior lobes. We used 12 mice for RNA seq experiments and 8 mice for RTqPCR validation.

RNAsequencing

RNA was extracted from dissected regions using TRIzol Reagent (Life Technologies). RNA was sent to the University of Minnesota Genomics Center for quality control, including quantification using fluorimetry (RiboGreen assay, Life Technologies), and RNA integrity with capillary electrophoresis (Agilent BioAnalyzer 2100, Agilent Technologies Inc.), generating an RNA integrity number (RIN). All submitted samples with RINs 8.0 or greater proceeded to RNA sequencing on an Illumina NextSeq 550 using a 100-nt paired-end read strategy [11]. Data is stored on University of Minnesota Supercomputing Institute Servers. To analyze data raw, paired short reads will be analyzed through CHURP (Collection of Hierarchical UMII-RIS Pipelines, PEARC ’19 Proceeding, Article No. 96), which includes data quality control via FastQC, data preprocessing via Trimmomatic [35], mapping via HiSat2 [36] against reference mouse genome and expression quantification via Subread [37]. Resulting count matrix of gene expression was used as input of R (https://www.r-project.org/) package: EdgeR [38][39] (v3.32.1), which tested the differential gene expression and visualized the behavior of expected invariant control genes and published positive control genes. EdgeR was used to reveal sample outliers through Multi-Dimensional Scaling (MDS) and Principle Component Analysis (PCA). Pathway analysis and dot plot creation was preformed using the clusterProfiler package (v3.18.1) using the top 500 DEGs based on absolute value of LogFC [40]. Heatmaps were created

using pheatmap package (https://CRAN.R-project.org/package=pheatmap)(v1.0.12) [X]. Volcano plots were created using BiocMananger (https://CRAN.R-project.org/package=BiocManager) (v1.30.16) and EnhancedVolcano (https://github.com/kevinblighe/EnhancedVolcano) (v1.8.0) packages.

RTqPCR

Total RNA was extracted from dissected mouse cerebellar regions - cerebellar cortex of the anterior vermis, cerebellar cortex of the posterior vermis, and the cerebellar cortex of hemispheres - using TRIzol (Life Technologies), and RT-qPCR was performed as described previously[41]. We used IDT Primetime primers for the following genes *Grid2* and *Gli1,* and 18S RNA was used for normalization.

Immunofluorescent (IF) staining IF was performed on minimum of six different floating 40-µm-thick brain slices from each mouse (six technical replicates per mouse per region or antibody of interest). Fluorescent images were acquired using an epifluorescent microscope (Leica DM6000) using a 20X objective. Single 20X images were stitched together to capture one plane of the entire mouse cerebellum. Confocal images were acquired using an Olympus FV10000 microscope using an oil 20X objective. Z-stacks consisting of twenty non-overlapping 1-µm-thick slices were taken of each stained brain slice per brain region (i.e., six z-stacks per mouse, each taken from a different brain slice). The laser power and detector gain were standardized and fixed between mice within a cohort, and all images for mice within a cohort were acquired in a single imaging session to allow for quantitative comparison.

We used primary antibodies against Purkinje cell marker calbindin (rabbit, Sigma-Aldrich, C9848) as previously described [42][43]. Quantitative analysis was performed using ImageJ (NIH) as described previously. To quantify relative intensity of staining for calbindin we measured the average signal intensity in the region of interest and normalized it to that of the WT mouse of that cohort. To quantify atrophy of the cerebellar molecular layer we took six measurements per image of the distance from the base of the Purkinje soma to the end of their dendrites, the average being the molecular layer width for that image. We used primary antibodies against vesicular glutamate transporter 2 (VGLUT2)

(guinea pig, Millipore, AB2251-I). Recession of climbing fibers was quantified by normalizing the width of VGLUT2 staining to the width of the molecular layer. We used primary antibodies for astrocytic marker glial fibrillary acidic protein (GFAP) (chicken, Millipore, AB5541. To quantify relative intensity of staining for GFAP we measured the average signal intensity in the region of interest and normalized it to that of the WT littermate mouse.

Statistical analysis

Wherever possible, sample sizes were calculated using power analyses based on the standard deviations from our previous studies, significance level of 5%, and power of 90%. Statistical tests were performed with GraphPad Prism 7.0. Data was analyzed using two-way ANOVA (to assess the impact of genotype and treatment) followed by post-hoc two-tailed, unpaired Student's t-test (to test statistical significance of differences between groups of interest wherein only one variable was different (treatment or genotype), or one-way ANOVA followed by the Sidak's post-hoc test. Outliers were determined using GraphPad PRISM's Robust regression and Outlier removal (ROUT) with a Q=1% for non-biased selection.

Data availability

All the data from this study are available from the authors.

Results

Cerebellar cortical pathology is heterogeneous in *Atxn1*$^{154Q/2Q}$ SCA1 knock-in mice

Recent studies have indicated significant regional diversity in the cerebellar cortex [22][23][44], particularly across anterior and posterior cerebellar lobules that can play a role in selective neuronal vulnerability in disease [45][46][47][48]. MRI and postmortem studies indicate worse pathology in posterior vermis and cerebellar hemispheres of patients with SCA1. To investigate whether these regional differences in cerebellar pathology are present in SCA1mouse models, we used SCA1 knock-in line *Atxn1*$^{154Q/2Q}$ wherein 154 CAG repeats are knocked-in to the endogenous mouse *Atxn1*

gene leading to endogenous levels and spatial pattern of mutant ATXN1 expression throughout the brain [28].

We examined cerebellar pathology at 12-weeks as at this time point, *Atxn1*$^{154Q/2Q}$ mice have already developed motor deficits seen in the rotarod test, dendritic atrophy and reactive gliosis. However, most studies have described these pathogenic changes only in the primary fissure of the cerebellar cortex (lobules V/VI). To assess whether SCA1 pathology was uniform across the cerebellar cortex, we examined four lobules of the cerebellar vermis – anterior lobule II, primary fissure lobules V/VI, and posterior lobules VII and X (Figure 1A). We stained sagittal cerebellar sections with PC marker Calbindin to assess PC health (Figure 1C). Thinning of the molecular layer (ML) and atrophy of the Purkinje cell (PC) dendrites area well described SCA1 pathology that are commonly used to quantify cerebellar degeneration in SCA1 mouse models [49][50]. When measuring molecular layer width, we found that while there was a reduction in all four of the lobules it was only significant in lobule V/VI (Figure 1 B). When we measured calbindin intensity, another method commonly used to assess PC health, we found that there was a significant reduction in lobules VII, and X and decrease was largest for lobule X (Figure 1 D). A loss of VGLUT2 synapses has been seen as PC dendrites undergo degeneration and can be quantified as the ratio of width of VGLUT2 staining in the ML and the width of the ML (Figure 1E). We found a statistically significant reduction in the VGLUT2/ML ratio in the lobules V/VI, VII, and X, but not in the anterior lobule II (Figure 1F). Thus, anterior lobule II showed no significant changes in any of our measures of PC pathology whereas more posterior lobules V/VI, VII and X showed a significant reduction in several measures of PC pathology with lobule X being most affected in CALB1 staining and VGLUT2/ML ratio, and lobules V/VI showed significant reduction in the thickness of molecular layer. This data taken together suggests that the degeneration of PCs in the cerebellar cortex is not uniform at 12-week time point and that there is some sparing of PC degeneration in the anterior region of the cerebellar vermis.

Additionally, we stained for GFAP, an astrocyte marker, to assess the level of astrogliosis at this time point across the cerebellar cortex of the vermis (Figure 1G). We found an increase in GFAP staining intensity only in lobule X, with no significant difference in the other lobules examined (Figure 1H). We also stained for Iba1, a microglial marker, to assess the number of microglia present in the molecular layer in each of these vermal lobules (Figure 1I). While we found no significant differences in Iba1 density in these vermal regions, there was a trending increase in Iba1 density in lobule X (Figure 1J). This result suggests that the level of gliosis is also different across the cerebellar cortex and that the posterior vermis may be more severely affected.

We confirmed these findings of non-uniform PC pathology across the cerebellum at slightly later time point at 18 weeks. Utilizing calbindin and measuring molecular layer thickness in each cerebellar lobule, we saw that lobule X was the most affected at this time point as well (Supplementary figure 1A-B). In the hemispheres all lobules had a decrease in molecular layer thickness that reached statistical significance only in Simple and Crus I (Supplementary figure 1C). These results suggest that cerebellar pathogenesis is heterogeneous in *Atxn1*$^{154Q/2Q}$ mice with posterior vermal cortex and cortex of the hemispheres being more affected than anterior vermal lobules.

Experimental design to identify gene expression differences across cerebellar regions in physiological conditions and in SCA1

Previous studies identified gene expression differences in neurons and glia across brain regions under physiological conditions and in neurodegeneration [51][52][53][2][54]. We reasoned that transcriptomic study of more vulnerable cerebellar regions (posterior vermis and hemispheres) and a relatively resistant anterior vermis could provide crucial insight into mutant ATXN1–dependent selective pathogenesis in SCA1. We employed a quick and reproducible dissection method [34] to isolate distinct cortical regions of the cerebellum: cerebellar cortex of the anterior vermis (CCAV),

cerebellar cortex of the posterior vermis (CCPV), and cerebellar cortex of the hemispheres (CCH) from seven SCA1 knock-in mice and five wild-type littermates at 18 weeks of age for a total of 36 samples (Figure 2A). While no sex-effects have been previously reported in SCA1 knock-in mice, studies have shown sex-differences in normal cerebellar physiology that can contribute to sex-specific mechanisms of disease pathogenesis [55]. For this reason, we designed our study to have equal number of female and male mice (N =6 of each).

We detected the expected pattern of expression of genes known to be differentially expressed across anterior and posterior cerebellum (Table 1). This included *Kcng4* that was previously shown to be enriched in the anterior vermis, and *Aldoc* which is known to be enriched in posterior vermis. As expected expression of *Kcng4* was 1.66 fold higher in anterior vermis (false discovery rate FDR = $5.6X10^{-9}$), while expression of *Aldoc* was 1.65 fold higher in posterior vermis (FDR =$3.96 X 10^{-5}$), thus validating the ability of our method (dissection and RNA extraction followed by RNAsequencing analysis) to detect intracerebellar differences in gene expression.

To understand what causes increased vulnerability of some neurons, it is important to identify their molecular signatures in physiological conditions as they may predispose them to increased sensitivity as well as their molecular responses to toxic mutant protein. Thereby, we designed our study to compare transcriptome of anterior vermis, posterior vermis and hemispheres in physiological conditions in wild-type mice (Figure 2B, yellow arrows) as well as transcriptome alterations in each of these regions in SCA1 mice (Figure 2B, red arrows). In both conditions we investigated the effect of sex.

Transcriptomic analysis in wild-type mice identifies differently regulated genes across anterior vermis and posterior vermis and hemispheres

Previous studies identified inherent differences between anterior and posterior cerebellum. For instance, cerebellar zonal patterning identified by zebrin II immunoreactivity is more uniform in

posterior lobules [56]. It has also been demonstrated that PCs have different firing patterns across the vermal lobules, with PCs in the anterior vermis demonstrating a higher tonic firing rate than PCs in the posterior vermis [23]. Given these naturally occurring differences, we examined differences in gene expression between anterior and posterior vermis, and hemispheres within wild-type mice.

We conducted comparisons of each cerebellar cortical region to each other resulting in 3 comparisons (Figure 2B, yellow arrows). Based on these comparisons we ranked the top 15 up and down regulated differentially expressed genes and normalized the counts for each gene across all WT samples generating heatmaps for each comparison (Figure 3A-C). These heatmaps highlight distinct differences in gene expression between each WT cerebellar cortical region.

For each comparison we identified the total number of differentially expressed genes. We identified 1229 genes that were differentially expressed in anterior vs posterior vermis in the wild-type mice. Most of these genes (884 or 71.9%) were expressed at higher level in the anterior vermis (Figure 3D). Comparison of transcripts in anterior vermis and hemispheres identified fewer differentially expressed genes (744) and, again, most were enriched in the anterior vermis compared to the hemispheres (Figure 3E). Interestingly, comparison of transcripts between the posterior vermis and hemispheres identified even fewer differentially expressed genes (365) (Figure 3F). These comparisons indicate higher molecular similarity between posterior vermis and hemispheres compared to anterior vermis which is consistent with their increased vulnerability. These results suggest that in the wild-type cerebellum the posterior vermis and hemispheres are the most similar cerebellar cortical regions and both regions are more distinct from the anterior vermis.

There are many specific genes that are differentially expressed in each of these cerebellar cortical regions that may point to potential mechanisms of protection or vulnerability. Genes enriched in anterior cerebellum include several genes known to provide neuroprotection. These genes include *Cck* and Cckbr involved in CCK (Cholesytokinin) signaling known to be protective in SCA1 and SCA2 [26][57]. Wnt signaling (*Wnt8*) [58] and neuropeptides *Vgf*, and *Sst* (somatostatin) [59][60] have each been implicated in neuroprotection in Alzheimer's disease, Parkinson's disease or ALS. In addition,

increased expression of genes encoding proteins with anti-inflammatory roles including neuropeptide Y receptors 1 and 5 (NPY1R and NPY5R)[61], and dopamine 2 receptor (*DRD2*) [62][63] also indicate increased protection against pro-inflammatory changes in the anterior vermis. As hypoxia was described in SCA1 mice, increased expression of *Ngb* (*neuroglobin*), gene that regulates oxygen availability in the anterior vermis may indicate increased protection against hypoxia in this region [64]. Intriguingly complement 3 (C3) that plays a role in developmental, physiological and pathological synaptic pruning is also enriched in anterior cerebellum[65][66].

On the other hand, several genes with higher expression in the posterior cerebellum could contribute to its increased vulnerability. These include, *Snca* (α*Synuclein*), intrinsic cell death mediator c*aspase-2*, and proinflammatory genes including *IL17Re* (*Interleukin 17 Receptor*), *Flt3l* (FMS-*like tyrosine kinase 3 ligand*), *NFAT* 5 *(nuclear factor of activated T cells 5*) and *Sp1*.

We also compared transcriptomes of female and male mice in each of these regions (Table 2). We have found very few DEG, and top ten were X and Y linked genes including *Ddx3y, Eif2s3Y, Xist, UtY, Kdm5d, Gm29650, Eif2s3, Ddx3x, Gm4017, Kdm6a, Kdm 5c*, validating our analysis. In the anterior vermis we identified four additional genes that were enriched in female anterior cerebellar vermis including *Sipa1l1 (Signal Induced Proliferation Associated 1 Like* 1) that was recently shown to be involved in synaptic GPCR signaling[67]. *Slc2a13* (solute carrier family 2 (facilitated glucose transporter) family 13) was also enriched in female posterior vermis and has been shown to play a role in regulation of cell signaling [68]. In the posterior vermis and cerebellar hemispheres, no additional DEGS were identified with more stringent FDR< 0.05, but there are several more genes that could be examined with a less stringent FDR threshold.

We also ran pathway analysis on the top 500 DEGs between cerebellar cortical regions ranked based on the absolute value of logFC and found that there are different enriched pathways between these cerebellar cortical regions in WT mice (Figure 3E). Notably the calcium signaling pathway and cAMP signaling pathway is enriched between the anterior and posterior vermis. Pathways of neurodegeneration are enriched between the anterior vermis and the posterior vermis and

hemispheres. KEGG analysis of genes enriched in posterior compared to anterior vermis identified axon guidance, PI3K-Akt signaling, AGE-RAGE signaling, ECM-receptor interaction and TGF Beta signaling as pathways characterizing posterior cerebellum (using gProfiler). On the other hand, KEGG analysis of genes enriched in the anterior cerebellum identified neuroactive ligand-receptor interaction, calcium signaling, synaptic vesicle cycle, and nicotine addiction as pathways characterizing anterior vermis (unsing gProfiler). While more examination will be necessary, this pathway analysis suggests there are inherently different molecular mechanisms that could predispose these regions to protection or vulnerability in disease.

SCA1 intracerebellar transcriptomics identifies shared and unique disease pathways

Next, we compared gene expression changes in SCA1 anterior and posterior vermis and hemispheres. We identified similar number of DEG in each of these regions (CCAV 1655, CCPV 1715 and CCH 1445). Approximately 42% (683) DEG were altered in all of the regions in the same direction constituting shared pathogenesis across the entire cerebellar cortex. The anterior vermis contained the most unique DEGs compared to the other regions, while the posterior vermis and hemispheres share many DEGs (Figure 5A). In each region the majority of the DEGs were down regulated in the *Atxn1*$^{154Q/2Q}$ mice (Figure 5B).

Heatmaps show the top 15 down and up regulated DEGs in each region, highlighting the heterogeneity in top dysregulated genes between the regions. As majority of the DEG are unique to each cerebellar cortical region, it is not surprising most of the top LogFC DEGs were unique to each region. However, there are a handful of DEGs that are shared across these regions. For instance, *Myo15*, *Ostn*, and *Car9* are down regulated in all cerebellar cortex regions of the *Atxn1*$^{154Q/2Q}$ mice. Not surprisingly they have all been found to be decreased in *Atxn1*$^{154Q/2Q}$ line using bulk RNA seq. *Myo15* encodes for the unconventional myosin and spontaneous mutations in this gene cause ataxia in rats [69]. *Car9* encodes for carbonic anhydrase 9, a transmembrane carbonic anhydrase isoform

that was found to play an important role in the regulation of the pH and inflammation and metabolism in cells of macrophage lineage [70][71].

Previous studies utilizing a transgenic mouse model of SCA1 found a module of genes related to Purkinje cell dysfunction labeled magenta genes. More recent studies found that these genes were also similarly affected in the *Atxn1*$^{154Q/2Q}$ mouse model based on bulk cerebellar analysis. After cerebellar dissection, we were able to assess these genes on a regional level. A subset of magenta genes are similarly down regulated in all regions of the cerebellar cortex (Supplemental Figure 2). This result suggests that this module of genes is affected across the cerebellar cortex.

From the heatmaps it is also clear to see that some of the top differentially expressed genes are unique to specific cerebellar cortical region. For example, *Wnt10b* is one of the top 15 downregulated genes only in the posterior vermis. Wnt signaling has been implicated as critical to Bergmann glia function [74]. Bergman glia interact closely with PC dendrites. This differential reduction in *Wnt10b* expression only in the posterior vermis could point to further underlying mechanisms in cerebellar cortical degeneration pattern[72][58]. Additionally, *tyrosine hydroxylase* (*Th*) the rate-limiting enzyme in the synthesis of catecholamines is in the top 15 down regulated genes only for the posterior vermis indicating dysregulated Th activity only in posterior cerebellum. This is significant considering cognitive impairments in *Atxn1*$^{154Q/2Q}$ mice and patients with SCA1 as Purkinje cell specific knock-out of *Th* impaired cognitive behaviors in mice [73].

Using the top 500 DEGs based on the absolute LogFC value in each cerebellar cortical region, we utilized pathway analyses to see which gene pathways are the most enriched in these regions. Using Gene Ontology (GO) databases for molecular function and biological pathways, we found many similarly enriched pathways across all three cerebellar cortical regions, including regulation of ion transmembrane transport, voltage gated channel activity, and potassium ion transmembrane transport. Many of these pathways have been identified in bulk cerebellar transcriptomic studies which validates our results (Sup fig 2).

When utilizing the KEGG database we found that there were many significantly enriched pathways that were unique only to the posterior vermis (Figure 5). For instance, there were multiple addiction pathways that were enriched only in the posterior vermis which could be related to the significant change in *Th* expression in the region. Wnt signaling pathway also uniquely enriched only in the posterior vermis. As mentioned previously Wnt signaling has been linked to Bergmann glia function and since Bergmann glia interact closely to PCs and function as signaling regulators this difference in pathway enrichment could point to a source of PC vulnerability in the posterior vermis[74]. The large number of unique pathways enriched in the posterior vermis of *Atxn1*$^{154Q/2Q}$ mice suggests possible mechanisms that underlie its vulnerability in SCA1 disease.

Cell-Specific differences across the cerebellar cortical regions

Based on the differences in the type of enriched pathways between the cerebellar cortical regions, in particular, the cell-signaling or ion channel pathways, we wanted to explore whether there are cell type specific differences in the cerebellar cortex in SCA1. In particular we investigated changes in the expression of genes critically important for the function of Purkinje cells and Bergmann glia.

We have found similar changes in the expression of Purkinje cell genes including potassium, calcium and sodium channels and glutamate receptors that were most pronounced in the posterior vermis (Figure 6A). We were most intrigued by *Grid2* (Glutamate Ionotropic Receptor Delta Type Subunit) which encodes a glutamate ionotropic receptor GRID2 that is highly expressed specifically in PCs. Lurcher point mutation (Lc) transforms the GRID2 receptor into a constitutively opened channel causing massive death of Purkinje cells in Lurcher mice [47]. Hotfoot (*Grid2ho/Grid2ho*) mice are “natural”*Grid2* knock-out mice and display ataxia and impaired motor learning [75], implicating importance of Grid2 for PC function and survival. In humans, a homozygous deletion in GRID2 causes cerebellar ataxia 18 [76][77]. Based on the RNAsequencing data, *Grid2* is significantly

decreased only in the posterior vermis and hemispheres but not in the anterior cerebellum (Figure 6C). We confirmed this result using an additional independent set of RNA isolated from these three regions and RTqPCR (Figure 6D). This difference in reduction in *Grid2* expression across the cerebellar cortex could point to its contribution to increased PC dysfunction and death in the posterior vermis and cerebellar hemispheres.

We examined the expression of a set of Bergmann glial genes in each cerebellar cortical region (Figure 6C). Expression of Bergmann glia marker gene *GFAP* was slightly decreased in the hemispheres and the anterior cerebellar vermis but not in the posterior vermis; while there was very slight decrease in another marker genes *S100B* and *Sox2* in all regions. This is consistent with increased BG gliosis in the posterior cerebellum along with likely slight loss of BG in all regions. BG homeostatic genes *Kcnj10* and *Slc1a3* were decreased in all regions, indicating decreased ability of BG to support PC function across cerebellum [78][79]. Importantly, BG in posterior cerebellum had most severe decrease in the expression of Shh receptors *Ptch1* and *Ptch2* and downstream transcriptional factor *Gli1* (Figure 6E). We have confirmed this decrease in Gli1 using RTqPCR on the independent set of RNA isolated from these three regions (Figure 6F). Since Shh signaling plays a key role in Purkinje cell-Bergmann glia communication [80] this result indicates that BG in posterior cerebellum are less responsive to PC signaling.

Discussion

Selective vulnerability of distinct neuronal populations is one of the key features of neurodegenerative diseases and as such studies have primarily focused on identifying mechanisms underlying pathogenesis in the most affected brain regions and cell types. Here we used comparative assessment of cellular and molecular differences between vulnerable and less affected tissues. We interrogated these differences in physiological and pathological state to provide insights into mechanisms that may predispose to disease and mediate increased pathogenesis in disease respectfully. In SCA1 the cerebellum, and specifically the Purkinje cells of the cerebellar cortex

undergo the most severe degeneration. Interestingly, imaging and postmortem studies demonstrated in patients with SCA1 that not all of the PCs undergo the same level of degeneration. In fact, there is evidence that the anterior region of the cerebellum is more spared from degeneration while the posterior vermis and cerebellar hemispheres appear to be more affected in patients with SCA1. The goals of this study were to investigate whether *Atxn1*$^{154Q/2Q}$ line of SCA1 knock-in mouse model copy this region specific vulnerability seen in patients so it can be used to identify the molecular mechanisms that underlie increased vulnerability or provide protection.

First, we found exacerbated degeneration of PCs and increased gliosis in the posterior cerebellar cortex of vermis in *Atxn1*$^{154Q/2Q}$ mice. In particular, we detected largest effect size and significance in excitatory synapse loss, PC atrophy, astro- and microgliosis in the posterior lobule X. On the other hand, lobule II in the anterior vermis did not exhibit any significant atrophy or gliosis. This pattern of PC degeneration matches the degeneration seen in human patients with SCA1 suggesting that this mouse model can be used to study the mechanisms underlying PC vulnerability in SCA1. Recently, two studies describe the opposite pattern of increased vulnerability in anterior vermis in Purkinje cell specific transgenic mouse model of SCA1, *Pcp2-ATXN1[82Q]* mice [81][82][83]. However, they have also found that relative sparing of posterior lobules is due to their low transgene expression in the posterior lobules of *Pcp2-ATXN1[82Q]* mice. Other models of diseases characterized by cerebellar degeneration have noted cerebellar regional differences in degeneration. In a study of Spinocerebellar Ataxia type 5 (SCA5) found that posterior lobules of the cerebellum were significantly vulnerable to disease [46]. This study found that the PC degeneration was related to the loss of normal glutamate transporter activity. Another disease associated with cerebellar degeneration is Niemann-Pick disease, typeC1 (NPC1). A study of NPC1 have found differential PC degeneration in which the posterior vermis is mostly protected from degeneration [45], this study found large transcriptomic differences between the anterior and posterior cerebellar vermis. The results of these studies and the work presented here highlight the importance of assessing the

pattern of degeneration across the cerebellum, as the region does not undergo degeneration in a uniform pattern.

In order to examine molecular mechanisms that may play a role in these cerebellar cortical regions, we utilized RNAsequencing analysis on cerebellar cortical regions of 18-week-old *Atxn1*$^{154Q/2Q}$ mice. With these results we were able to assess differences within the WT cerebellar cortical regions. We found broad differences in the top differentially expressed genes in each region, and noted that the anterior vermis has the most distinct differentially expressed genes (Figure 3A-F). One such inherent expression difference across the cerebellar cortex was that of *Cck* (Cholesytokinin) with higher expression in the anterior vermis. A recent study suggested that the expression of cck and its receptor can be protective against Purkinje cell degeneration in a transgenic model of SCA1[57]. This result paired with our findings could suggest a potential pathway for protection in the anterior vermis of *Atxn1*$^{154Q/2Q}$. Additionally, Tyrosine Hydroxylase (Th) expression is more highly expressed in the posterior vermis compared to the anterior regions. A recent study found that knocking out Th in these PCs leads to the development of a variety of cognitive deficits [75]. Given that the posterior vermis undergoes more severe degeneration in these *Atxn1*$^{154Q/2Q}$ mice, it is possible that the loss of Th positive neurons could play a role in cognitive deficits in these mice.

We also assessed differences between sexes. While the majority of the DEGs we chromosomal linked, we found a subset of genes that were more highly expressed in females *Atxn1*$^{154Q/2Q}$ mice based on sex (Table 2), and these genes will be further explored as potential targets for sex differences that underlie disease progression. Previous work has shown that sex-differences in normal cerebellar physiology that can play a role in sex-specific disease pathogenesis mechanisms [55]. In this work, we found that *Slc2a13* (solute carrier family 2 (facilitated glucose transporter) family 13) was enriched in the posterior vermis of female mice. *Slc2a13* has been shown to play a role in cell signaling [68]. These inherent differences in cerebellar physiology between sexes, could play a role in slightly different pathogenesis mechanisms in female and male

Atxn1$^{154Q/2Q}$ mice. Sex differences are a critical avenue to explore given that sex differences in disease progression could have a significant impact on the effectiveness of potential treatments.

Next we identified differentially expressed genes (DEGs) and molecular pathways in the *Atxn1*$^{154Q/2Q}$ mice. Overall, we found that the anterior vermis had the most unique DEGs (40%) (Figure 4A). We also noted high level of heterogeneity in the top differentially expressed genes in each region (Figure 4C-E). Additionally, pathway analysis with the top 500 DEGs in each region identified several pathways that were unique to the posterior vermis (Figure 5). Of note many of these pathways are related to addiction including cocaine, amphetamine, and nicotine addiction pathways. These pathways could be enriched in this region because of the increased expression of tyrosine hydroxylase (Th) in the posterior vermis. We know from previous work that Th positive PCs have an impact on a variety of cognitive behaviors [75]. Understanding the molecular pathways that could underlie this behavior would provide insight into the impact of the activity in the posterior vermis. Another uniquely impacted pathway in the posterior vermis was the Wnt signaling pathway. A recent study of Wnt-β-catenin signaling in SCA1 mice found that Bergmann glia are more affected by changes in Wnt signaling pathways [74]. As Bergmann glia interact very closely with PC dendrites, any dysfunction in BGs has a downstream impact on PC activity.

Given that many cell-signaling pathways were differentially enriched in the posterior vermis, that Purkinje cells form the main output of the cerebellar cortex, and that Bergmann glia interact closely with PCs we wanted to examine a subset of PC and BG specific genes to examine differences across the cerebellar cortex. For PCs, we focused in specifically on *Grid2* because of mouse genetic studies pointing to its important role in the cerebellar functioning and because mutations in *Grid2* cause ataxia in human patients [47][75][76][77]. In *Atxn1*$^{154Q/2Q}$ mice *Grid2* is significantly downregulated in the posterior vermis and cerebellar hemispheres, while the anterior vermis is spared. Knowing that loss of Grid2 function is connected to the development of ataxia in humans and mice, this result suggests a possible mechanism for increased vulnerability of PC in the posterior vermis n SCA1.

In addition, Bergmann glia are key for PC function and we have found alterations in Bergmann glia-Purkinje cell communication in the posterior vermis. Gli1 is a transcription factor induced by Shh signaling that is highly expressed in Bergmann glia and is critical for their function. We found that there was a significant reduction in the expression of *Gli1* in the posterior vermis and cerebellar hemispheres while the anterior vermis was less affected. Since Shh signaling plays a key role in PC-BG communication [80] this result indicates PC-BG signaling may be disrupted more significantly in the posterior vermis or cerebellar hemispheres. This difference again highlights a potential mechanism for SCA1 vulnerability in the posterior vermis.

Overall we hope that our data will be a rich resource to explore the regional differences in cerebellar degeneration in *Atxn1*$^{154Q/2Q}$ mice. Ideally this work will shed light on protective mechanisms that could be utilized to discover potential treatments or identify pathways that lead to tissue vulnerability and provide targets for treatments.

Figure legends

Figure 1. Assessment of dendritic atrophy, synaptic loss, and gliosis in four vermal regions in 12-week-old *Atxn1*$^{154Q/2Q}$ mice. A. Schematic of sagittal section of mouse cerebellar vermis from Allan Brain Atlas. Lobules measured highlighted in red boxes; Lobule II, V/VI, VII, and X. **B**. Measurement of molecular layer thickness of the four vermal lobules noted in A. n = 3-4 WT (black bars), 4-5 *Atxn1*$^{154Q/2Q}$ (pink bars), unpaired t-test, * = $p < 0.05$. **C**. Representative calbindin IHC images of lobule II (top) and X (bottom) for WT (left) and *Atxn1*$^{154Q/2Q}$ (right); used to measure molecular layer width and calbindin intensity. **D**. Calbindin staining intensity measurements in the four vermal lobule regions. n = 3-4 WT (black bars), 4-5 *Atxn1*$^{154Q/2Q}$ (pink bars), unpaired t-test, * = $p < 0.05$. **E**. Representative Calbindin and VGLUT2 IHC images of lobule II and X, WT (top) and *Atxn1*$^{154Q/2Q}$ (bottom), Calbindin staining (left), VGLUT2 staining (middle), merged images (right). Images used to take ratio measurement between molecular layer width and VGLUT2 puncta width. **F.** Molecular layer width/VGLUT2 puncta ratio measurements n the four vermal lobule regions. n = 3-4

WT (black bars), 4-5 *Atxn1*$^{154Q/2Q}$ (pink bars), unpaired t-test, * = $p < 0.05$, ** = $p < 0.005$. **G.** Representative GFAP IHC images of lobule II (top) and X (bottom) for WT (left) and *Atxn1*$^{154Q/2Q}$ (right); used to measure intensity of GFAP staining normalized to WT images. **H**. GFAP staining intensity measurements in the four vermal lobule regions. n = 4-5 WT (black bars), 6-7 *Atxn1*$^{154Q/2Q}$ (pink bars), unpaired t-test, * = $p < 0.05$. **I**. Representative Iba1 IHC images of lobule II (top) and X (bottom) for WT (left) and *Atxn1*$^{154Q/2Q}$ (right); used to measure density of microglia in molecular layer. **J.** Iba1 density measurements in molecular layer of four vermal lobule regions. n = 3 WT (black bars), 4 *Atxn1*$^{154Q/2Q}$ (pink bars), unpaired t-test.

Figure 2. Cerebellar dissection and RNAsequencing analysis method. A. Cartoon of cerebellar dissection and separate tissue for RNA extraction. Cerebellar vermis sections dissected into anterior (CCAV) and posterior regions (CCPV). Deep cerebellar nuclei punched out to save cerebellar cortex of hemispheres (CCH). Tissue from each region collected and saved separately. RNA extracted from each region separately to be used for RNAsequencing and RTqPCR. **B.** Schematic of RNAsequencing analysis method. Comparisons between WT and *Atxn1*$^{154Q/2Q}$ mice in each cerebellar cortical region (red arrows) producing differentially expressed genes (DEGs) in *Atxn1*$^{154Q/2Q}$ mice. Comparisons within WT cerebellar cortical regions (yellow arrows) producing DEGs between each cerebellar cortical region.

Figure 3. Transcriptomic analysis in wild-type mice identifies differently regulated genes across the cerebellar cortex. A-C Heatmaps of top up and down regulated DEGs in between the anterior and posterior vermis (A), the anterior vermis and the cerebellar hemispheres (B), and the posterior vermis and cerebellar hemispheres (C). Heatmaps were generated by ranking the top 15 up and down regulated DEGs based on logFC value and plotting the counts of each gene in individual samples. Expression is normalized per gene in the heat map representation. **D-F** Volcano plots of all DEGs between the anterior and posterior vermis (D), the anterior vermis and the cerebellar

hemispheres (E), and the posterior vermis and cerebellar hemispheres (F). Red dots represent significant DEGs based on p-value and logFC, gray dots represent DEGs only significant by one metric or that did not reach significance. **G.** KEGG pathway analysis of enriched pathways of top 500 DEGs between the anterior and posterior vermis, the anterior vermis and the cerebellar hemispheres, and the posterior vermis and cerebellar hemispheres. Dot size represents number of genes in the enriched pathway, and color of the dot represents p-value.

Figure 4. SCA1 intracerebellar transcriptomics identifies shared and unique disease pathways in *Atxn1*$^{154Q/2Q}$ mice. A. Venn diagram of DEGs in each cerebellar cortical region. 1655 DEGs in CCAV (green), 1755 DEGs in CCPV (purple), and 1444 DEGs in CCH (blue). **B.** Up and down regulated DEGs in CCAV, CCPV, and CCH. **C-E.** Heatmaps of top up and down regulated DEGs in between WT and *Atxn1*$^{154Q/2Q}$ mice in each cerebellar cortical region: CCAV (C), CCPV (D), and CCH (E). Each column represents an individual sample, WT in pink, *Atxn1*$^{154Q/2Q}$ in teal, females with hashed boxes, males with solid boxes. Heatmaps were generated by ranking the top 15 up and down regulated DEGs based on logFC value and plotting the counts of each gene in individual samples. Expression is normalized per gene in the heat map representation.

Figure 5. Enriched pathway analysis of cerebellar cortical regions. KEGG pathway analysis of enriched pathways of top 500 DEGs between WT and *Atxn1*$^{154Q/2Q}$ mice in each cerebellar cortical region. Dot size represents number of genes in the enriched pathway, and color of the dot represents p-value.

Figure 6. Cell-specific gene expression across the cerebellar cortical regions. A. Purkinje cell specific signaling gene expression differences in *Atxn1*$^{154Q/2Q}$ mice based on logFC across each cerebellar cortical region; anterior vermis (left), posterior vermis (middle), cerebellar hemispheres (right). **B.** Bergmann glial specific gene expression differences in *Atxn1*$^{154Q/2Q}$ mice based on logFC

across each cerebellar cortical region; anterior vermis (left), posterior vermis (middle), cerebellar hemispheres (right). *Grid2* expression from RNAsequencing results across cerebellar cortical regions; red bars mark significant logFC based on $p < 0.05$, black bars mark not significant logFC based on $p > 0.05$. **D.** *Grid2* mRNA expression across cerebellar cortical regions in WT and *Atxn1*$^{154Q/2Q}$ mice by RTqPCR. WT in black bars, *Atxn1*$^{154Q/2Q}$ in pink bars. N = 4 per genotype. Error bars SEM, Welchs t-test, * = $p < 0.05$. **E.** *Gli1* expression from RNAsequencing results across cerebellar cortical regions; red bars mark significant logFC based on $p < 0.05$, black bars mark not significant logFC based on $p > 0.05$. **F.** *Gli1* mRNA expression across cerebellar cortical regions in WT and *Atxn1*$^{154Q/2Q}$ mice by RTqPCR. WT in black bars, *Atxn1*$^{154Q/2Q}$ in pink bars. N = 4 per genotype. Error bars SEM, Welchs t-test, * = $p < 0.05$, ** = $p<0.005$.

Table 1. RNAsequencing results of genes known to be differentially expressed across anterior and posterior cerebellum. *Aldolase C* is known to be more highly expressed in the posterior vermis, while *Kcng4* has been shown to be more highly expressed in the anterior vermis. The RNAsequencing data show an expected fold change for both genes at a significant false discovery rate (FDR).

Table 2. Transcriptomic analysis of sex differences in *Atxn1*$^{154Q/2Q}$ mice across cerebellar cortical regions. Table of DEGs between sexes in each cerebellar cortical region. Listed by logFC value associated with each gene. Majority of genes were X and Y chromosome linked but genes highlighted in yellow are not associated with sex chromosomes. They are more highly expressed in the female anterior vermis.

Supplementary Figure 1. Molecular layer thickness decrease is not uniform across cerebellar vermis and hemisphere in 18-week-old *Atxn1*$^{154Q/2Q}$ mice A. Sections from 18 weeks old *Atxn1*$^{154Q/2Q}$ mice and wild-type controls were stained for calbindin, marker of Purkinje cells. Wide

field images were acquired using an epifluorescent microscope (Leica DM6000B). WT images (top), *Atxn1*$^{154Q/2Q}$ (bottom), vermis sections (left), hemisphere sections (right). Quantification of the molecular layer width in vermis (**B**) and hemispheres (**C**). N=4 per genotype, WT in black bars, *Atxn1*$^{154Q/2Q}$ in pink bars, data is presented as Mean ±SEM, 2 Way ANOVA with Sidaak's post hoc test. * = $p<0.05$, **** = $p<0.0001$.

Supplementary Figure 2. Alteration in gene expression of genes found to be associated with Purkinje cell dysfunction across regions of the cerebellar cortex in *Atxn1*$^{154Q/2Q}$ mice. Assessed logFC of a subset of genes found to be associated with PC dysfunction in a transgenic mouse model of SCA1, designated magenta genes, in each region of the cerebellar cortex in *Atxn1*$^{154Q/2Q}$ mice. Red bars indicate significant logFC based on $p < 0.05$.

Supplementary Figure 3. GO pathway analysis of differentially expressed genes across cerebellar cortical regions in *Atxn1*$^{154Q/2Q}$ mice. A. Enriched pathways based on GO: Biological process. **B**. Enriched pathways based on GO: Molecular Function. For each analysis, the top 500 DEGs based on absolute value of logFC between WT and *Atxn1*$^{154Q/2Q}$ mice in each cerebellar cortical region were run through the GO database. Most pathways were enriched in all cerebellar cortical regions. Dot size represents number of genes in the enriched pathway, and color of the dot represents p-value.

References

1. Roselli F, Caroni P. From intrinsic firing properties to selective neuronal vulnerability in neurodegenerative diseases. Neuron [Internet]. Elsevier Inc.; 2015;85:901–10. Available from: http://dx.doi.org/10.1016/j.neuron.2014.12.063

2. Saxena S, Caroni P. Selective Neuronal Vulnerability in Neurodegenerative Diseases: From

Stressor Thresholds to Degeneration. Neuron [Internet]. Elsevier Inc.; 2011;71:35–48. Available from: http://dx.doi.org/10.1016/j.neuron.2011.06.031

3. Friedrich J, Kordasiewicz HB, O'Callaghan B, Handler HP, Wagener C, Duvick L, et al. Antisense oligonucleotide–mediated ataxin-1 reduction prolongs survival in SCA1 mice and reveals disease-associated transcriptome profiles. JCI Insight. 2018;

4. Driessen TM, Lee PJ, Lim J. Molecular pathway analysis towards understanding tissue vulnerability in spinocerebellar ataxia type 1. Elife. 2018;1–32.

5. Orr HT, Chung MY, Banfi S, Kwiatkowski TJ Jr, Servadio A, Beaudet AL, McCall AE, Duvick LA, Ranum LP ZH. Expansion of an unstable trinucleotide CAG repeat in spinocerebellar ataxia type 1. Nat Genet. 1993;4:221.

6. Zoghbi HY, Orr HT. Pathogenic mechanisms of a polyglutamine-mediated neurodegenerative disease, Spinocerebellar ataxia type 1. J. Biol. Chem. 2009;284:7425–9.

7. Seidel K, Siswanto S, Brunt ERP, Den Dunnen W, Korf HW, Rüb U. Brain pathology of spinocerebellar ataxias. Acta Neuropathol. 2012;124:1–21.

8. I. K, M. M, T. S-H, M. H, T. K, U. W, et al. Neuropsychological features of patients with spinocerebellar ataxia (SCA) types 1, 2, 3, and 6. Cerebellum. 2010;9:433–42.

9. Zoghbi HY, Pollack MS, Lyons SLA, Ferrell TRE, Daiger SP, Beaudet AL. Spinocerebellar Ataxia□: Variable Age of Onset and Linkage to Human Leukocyte Antigen in a Large Kindred. Ann. Neurol. 1988;23:580–4.

10. Koeppen AH. The pathogenesis of spinocerebellar ataxia. The cerebellum. 2005;4:62–73.

11. Friedrich J, Henzler C, Orr HT, Friedrich J, Kordasiewicz HB, Callaghan BO, et al. Antisense oligonucleotide–mediated ataxin-1 reduction prolongs survival in SCA1 mice and reveals disease-associated transcriptome profiles. J. Clin. Investig. 2018;3.

12. Paulson HL, Shakkottai VG, Clark HB, Orr HT. Polyglutamine spinocerebellar ataxias-from genes to potential treatments. Nat. Rev. Neurosci. 2017.

13. Rüb U, Schöls L, Paulson H, Auburger G, Kermer P, Jen JC, et al. Clinical features,

neurogenetics and neuropathology of the polyglutamine spinocerebellar ataxias type 1, 2, 3, 6 and 7. Prog. Neurobiol. 2013.

14. Rüb U, Bürk K, Timmann D, den Dunnen W, Seidel K, Farrag K, et al. Spinocerebellar ataxia type 1 (SCA1): New pathoanatomical and clinico-pathological insights. Neuropathol. Appl. Neurobiol. 2012;38:665–80.

15. Tedesco AM, Chiricozzi FR, Clausi S, Lupo M, Molinari M, Leggio MG. The cerebellar cognitive profile. Brain. 2011;134:3672–86.

16. Koziol LF, Budding D, Andreasen N, Arrigo SD, Schmahmann J, Vandervert L, et al. Consensus Paper□: The Cerebellum ' s Role in Movement and Cognition. Cerebellum. 2014;13:151–77.

17. D'Mello AM, Stoodley CJ. Cerebro-cerebellar circuits in autism spectrum disorder. Front. Neurosci. 2015;9.

18. Buckner RL, Krienen FM, Castellanos A, Diaz JC, Yeo BTT. The organization of the human cerebellum estimated by intrinsic functional connectivity. J. Neurophysiol. 2011;106:2322–45.

19. Middleton F a, Strick PL. Anatomical evidence for cerebellar and basal ganglia involvement in higher cognitive function. Science (80-.). 1994;266:458–61.

20. Shakkottai VG, Batla A, Bhatia K, Dauer WT, Dresel C, Niethammer M, et al. Current Opinions and Areas of Consensus on the Role of the Cerebellum in Dystonia. Cerebellum [Internet]. The Cerebellum; 2016;1–18. Available from: http://dx.doi.org/10.1007/s12311-016-0825-6

21. Choe KY, Sanchez CF, Harris NG, Otis TS, Mathews PJ. Optogenetic fMRI and electrophysiological identification of region-specific connectivity between the cerebellar cortex and forebrain. Neuroimage [Internet]. Elsevier Ltd; 2018;173:370–83. Available from: https://doi.org/10.1016/j.neuroimage.2018.02.047

22. Kozareva V, Martin C, Osorno T, Rudolph S, Guo C, Vanderburg C, et al. A transcriptomic atlas of the mouse cerebellum reveals regional specializations and novel cell types. BioRxiv. 2020;

23. Zhou H, Lin Z, Voges K, Ju C, Gao Z, Bosman LWJ, et al. Cerebellar modules operate at different frequencies. Elife. 2014;1–18.

24. Reetz K, Costa AS, Mirzazade S, Lehmann A, Juzek A, Linnemann C, et al. Genotype-specific patterns of atrophy progression are more sensitive than clinical decline in SCA1, SCA3 and SCA6. Brain. 2013;136:905–17.

25. Nigri A, Sarro L, Mongelli A, Castaldo A, Porcu L, Pinardi C, et al. Spinocerebellar Ataxia Type 1□: One □ Year Longitudinal Study to Identify Clinical and MRI Measures of Disease Progression in Patients and Presymptomatic Carriers. The Cerebellum [Internet]. Springer US; 2021; Available from: https://doi.org/10.1007/s12311-021-01285-0

26. Ingram M, Wozniak EAL, Duvick L, Yang R, Bergmann P, Carson R, et al. Cerebellar Transcriptome Profiles of ATXN1 Transgenic Mice Reveal SCA1 Disease Progression and Protection Pathways. Neuron [Internet]. Elsevier Inc.; 2016;89:1194–207. Available from: http://linkinghub.elsevier.com/retrieve/pii/S0896627316001045

27. Paulson HL, Shakkottai VG, Clark HB, Orr HT. Polyglutamine spinocerebellar ataxias — from genes to potential treatments. Nat. Rev. Neurosci. [Internet]. Nature Publishing Group; 2017;18:613–26. Available from: http://dx.doi.org/10.1038/nrn.2017.92

28. Watase K, Weeber EJ, Xu B, Antalffy B, Yuva-Paylor L, Hashimoto K, et al. A long CAG repeat in the mouse Sca1 locus replicates SCA1 features and reveals the impact of protein solubility on selective neurodegeneration. Neuron. 2002;34:905–19.

29. Burright EN, Clark HB, Servadio a, Matilla T, Feddersen RM, Yunis WS, et al. SCA1 transgenic mice: a model for neurodegeneration caused by an expanded CAG trinucleotide repeat. Cell. 1995;82:937–48.

30. Ingram M, Wozniak EAL, Duvick L, Zoghbi HY, Henzler C, Orr HT. Cerebellar Transcriptome Profiles of ATXN1 Transgenic Mice Reveal SCA1 Disease Progression and Protection Pathways Article Cerebellar Transcriptome Profiles of ATXN1 Transgenic Mice Reveal SCA1 Disease Progression and Protection Pathways. Neuron [Internet]. Elsevier Inc.; 2016;89:1194–207. Available from: http://dx.doi.org/10.1016/j.neuron.2016.02.011

31. Duvick L, Barnes J, Ebner B, Agrawal S, Andresen M, Lim J, et al. SCA1-like disease in mice

expressing wild-type Ataxin-1 with a serine to aspartic acid replacement at residue 776. Neuron [Internet]. Elsevier Inc.; 2010;67:929–35. Available from: http://dx.doi.org/10.1016/j.neuron.2010.08.022

32. Ruegsegger C, Stucki DM, Steiner S, Angliker N, Radecke J, Keller E, et al. Impaired mTORC1-Dependent Expression of Homer-3 Influences SCA1 Pathophysiology. Neuron. 2016;89:129–46.

33. National Research Council (US) Committee for the Update of the Guide for the Care and Use of Laboratory Animals. Guide for the Care and Use of Laboratory Animals, 8th edition. 2011.

34. Hamel KA, Cvetanovic M. Cerebellar Regional Dissection for Molecular Analysis. JOVE. 2021;1–16.

35. Bolger AM, Lohse M, Usadel B. Genome analysis Trimmomatic□: a flexible trimmer for Illumina sequence data. Bioinformatics. 2014;30:2114–20.

36. Kim D, Langmead B, Salzberg SL. HISAT: a fast spliced aligner with low memory requirements. Nat Methods. 2015;12:357–60.

37. Liao Y, Smyth GK, Shi W. featureCounts□: an efficient general purpose program for assigning sequence reads to genomic features. Bioinformatics. 2014;30:923–30.

38. Love MI, Huber W, Anders S. Moderated estimation of fold change and dispersion for RNA-seq data with DESeq2. Genome Biol. 2014;15:1–21.

39. Chen Y, Lun ATL, Smyth GK. From reads to genes to pathways: Differential expression analysis of RNA-Seq experiments using Rsubread and the edgeR quasi-likelihood pipeline. F1000Research. 2016;5:1–51.

40. Yu G, Wang LG, Han Y, He QY. ClusterProfiler: An R package for comparing biological themes among gene clusters. Omi. A J. Integr. Biol. 2012;16:284–7.

41. Rosa J, Hamel K, Sheeler C, Borgenheimer E, Soles A, Ghannoum F, et al. Early stage of Spinocerebellar Ataxia Type 1 (SCA1) progression exhibits region- and cell-specific pathology and is partially ameliorated by Brain Derived Neurotrophic Factor (BDNF). BioRxiv. 2021;1:doi: https://doi.org/10.1101/2021.09.13.460129□;

42. Kim JH, Lukowicz A, Qu W, Johnson A, Cvetanovic M. Astroglia contribute to the pathogenesis of spinocerebellar ataxia Type 1 (SCA1) in a biphasic , stage-of-disease specific manner. Glia. 2018;1–16.

43. Asher M, Johnson A, Zecevic B, Pease D, Cvetanovic M. Ataxin-1 regulates proliferation of hippocampal neural precursors. Neuroscience [Internet]. IBRO; 2016;322:54–65. Available from: http://dx.doi.org/10.1016/j.neuroscience.2016.02.011

44. Kim C, Oh S, Lee JH, Chang SO, Kim J, Kim SJ. Lobule-specific membrane excitability of cerebellar Purkinje cells. J Physiol. 2012;2:273–88.

45. Martin KB, Williams IM, Cluzeau C V, Cougnoux A, Dale RK, Iben JR, et al. Identification of Novel Pathways Associated with Patterned Cerebellar Purkinje Neuron Degeneration in Niemann-Pick Disease , Type C1. Int. J. Mol. Sci. 2020;21.

46. Perkins EM, Suminaite D, Clarkson YL, Lee SK, Lyndon AR, Rothstein JD, et al. Posterior cerebellar Purkinje cells in an SCA5/SPARCA1 mouse model are especially vulnerable to the synergistic effect of loss of β-III spectrin and GLAST. Hum. Mol. Genet. [Internet]. 2016;25:ddw274-. Available from: http://hmg.oxfordjournals.org/cgi/content/long/ddw274v2%5Cnhttp://www.hmg.oxfordjournals.org/lookup/doi/10.1093/hmg/ddw274

47. Sarna JR, Hawkes R. Patterned Purkinje cell death in the cerebellum. 2003.

48. Stoyas CA, Bushart DD, Switonski PM, Auwerx J, Shakkottai VG, Spada AR La, et al. Restores Calcium Homeostasis to Achieve Neuroprotection in Spinocerebellar Ataxia Type 7 Article Nicotinamide Pathway-Dependent Sirt1 Activation Restores Calcium Homeostasis to Achieve Neuroprotection in Spinocerebellar Ataxia Type 7. Neuron [Internet]. Elsevier Inc.; 2020;105:630-644.e9. Available from: https://doi.org/10.1016/j.neuron.2019.11.019

49. Ebner B, Ingram MA, Barnes JA, Duvick LA, Frisch JL, Clark HB, et al. Purkinje cell ataxin-1 modulates climbing fiber synaptic input in developing and adult mouse cerebellum. J. Neurosci. [Internet]. 2013;33:5806–20. Available from: http://www.ncbi.nlm.nih.gov/pubmed/23536093

50. Kim JH, Lukowicz A, Qu W, Johnson A, Cvetanovic M. Astroglia contribute to the pathogenesis of spinocerebellar ataxia Type 1 (SCA1) in a biphasic, stage-of-disease specific manner. Glia. 2018;66:1972–87.

51. Ayata P, Badimon A, Strasburger HJ, Duff MK, Montgomery SE, Loh YE, et al. Epigenetic regulation of brain region-specific microglia clearance activity. Nat. Neurosci. [Internet]. 2018;21:1049–60. Available from: http://dx.doi.org/10.1038/s41593-018-0192-3

52. Soreq L, Brain UKC, North American BE, Rose J, Patani R, Ule J. Major Shifts in Glial Regional Identity Are a Transcriptional Hallmark of Human Brain Aging. CellReports [Internet]. ElsevierCompany.; 2017;18:557–70. Available from: http://dx.doi.org/10.1016/j.celrep.2016.12.011

53. Grabert K, Michoel T, Karavolos MH, Clohisey S, Baillie JK, Stevens MP, et al. Microglial brain region − dependent diversity and selective regional sensitivities to aging. Nat Neurosci. 2016;19:504.

54. Cragnolini A, Lampitella G, Virtuoso A, Viscovo I, Panetsos F, Papa M, et al. Regional brain susceptibility to neurodegeneration: What is the role of glial cells? Neural Regen. Res. 2020;15:838–42.

55. Mercer AA, Palarz KJ, Tabatadze N, Woolley CS, Raman IM. Sex differences in cerebellar synaptic transmission and sex-specific responses to autism-linked Gabrb3 mutations in mice. Elife. 2016;5.

56. Sillitoe R V, Fu Y, Watson C. Cerebellum [Internet]. Mouse Nerv. Syst. Elsevier Inc.; 2012. Available from: http://dx.doi.org/10.1016/B978-0-12-369497-3.10011-1

57. Wozniak EAL, Chen Z, Paul S, Yang P, Figueroa KP, Friedrich J, et al. Cholecystokinin 1 receptor activation restores normal mTORC1 signaling and is protective to Purkinje cells of SCA mice. Cell Rep. [Internet]. ElsevierCompany.; 2021;37:109831. Available from: https://doi.org/10.1016/j.celrep.2021.109831

58. Palomer E, Buechler J, Salinas PC. Wnt signaling deregulation in the aging and Alzheimer's brain. Front. Cell. Neurosci. 2019;13:1–8.

59. Quinn JP, Kandigian SE, Trombetta BA, Arnold SE, Carlyle BC. VGF as a biomarker and

therapeutic target in neurodegenerative and psychiatric diseases. Brain Commun. 2021;3.

60. Song YH, Yoon J, Lee SH. The role of neuropeptide somatostatin in the brain and its application in treating neurological disorders. Exp. Mol. Med. [Internet]. Springer US; 2021;53:328–38. Available from: http://dx.doi.org/10.1038/s12276-021-00580-4

61. Li C, Wu X, Liu S, Zhao Y, Zhu J, Liu K. Roles of Neuropeptide Y in Neurodegenerative and Neuroimmune Diseases. Front. Neurosci. 2019;13:1–11.

62. Zhu J, Sun T, Zhang J, Liu Y, Wang D, Zhu H, et al. Drd2 biased agonist prevents neurodegeneration against NLRP3 inflammasome in Parkinson's disease model via a β-arrestin2-biased mechanism. Brain. Behav. Immun. [Internet]. Elsevier; 2020;90:259–71. Available from: https://doi.org/10.1016/j.bbi.2020.08.025

63. Du RH, Zhou Y, Xia ML, Lu M, Ding JH, Hu G. α-Synuclein disrupts the anti-inflammatory role of Drd2 via interfering β-arrestin2-TAB1 interaction in astrocytes. J. Neuroinflammation. Journal of Neuroinflammation; 2018;15:1–13.

64. Cvetanovic M, Patel JM, Marti HH, Kini AR, Opal P. Vascular endothelial growth factor ameliorates the ataxic phenotype in a mouse model of spinocerebellar ataxia type 1. Nat. Med. [Internet]. 2011;17:1445–7. Available from: http://www.pubmedcentral.nih.gov/articlerender.fcgi?artid=3287040&tool=pmcentrez&rendertype=abstract

65. Hammond TR, Robinton D, Stevens B. Microglia and the Brain□: Complementary Partners in Development and Disease. Annu. Rev. Cell Dev Biol. 2018;1–22.

66. Stephan AH, Barres B a., Stevens B. The Complement System: An Unexpected Role in Synaptic Pruning During Development and Disease. Annu. Rev. Neurosci. 2012;35:369–89.

67. Matsuura K, Kobayashi S, Konno K, Yamasaki M, Horiuchi T, Senda T, et al. SIPA1L1/SPAR1 is a non-PSD protein involved in GPCR signaling. bioRxiv. 2021;

68. Li CY, Ou RW, Chen YP, Gu XJ, Wei QQ, Cao B, et al. Mutation analysis of seven SLC family transporters for early-onset Parkinson's disease in Chinese population. Neurobiol. Aging [Internet].

Elsevier Inc.; 2021;103:152.e1-152.e6. Available from: https://doi.org/10.1016/j.neurobiolaging.2021.02.022

69. Held N, Smits BMG, Gockeln R, Schubert S, Nave H, Northrup E, et al. A mutation in MYo15 leads to Usher-like symptoms in LEW/Ztm-ci2 rats. PLoS One. 2011;6.

70. Demandt JAF, Dubois LJ, van Kuijk K, Zaťovičová M, Jin H, Parkkila S, et al. The hypoxia-sensor carbonic anhydrase IX affects macrophage metabolism, but is not a suitable biomarker for human cardiovascular disease. Sci. Rep. [Internet]. Nature Publishing Group UK; 2021;11:1–14. Available from: https://doi.org/10.1038/s41598-020-79978-5

71. Henry EK, Sy CB, Inclan-Rico JM, Espinosa V, Ghanny SS, Dwyer DF, et al. Carbonic anhydrase enzymes regulate mast cell-mediated inflammation. J. Exp. Med. 2016;213:1663–73.

72. Lordkipanidze T, Dunaevsky A. Purkinje cell dendrites grow in alignment with Bergmann glia. Glia. 2005;51:229–34.

73. Locke TM, Fujita H, Hunker A, Johanson SS, Darvas M, du Lac S, et al. Purkinje Cell-Specific Knockout of Tyrosine Hydroxylase Impairs Cognitive Behaviors. Front. Cell. Neurosci. 2020;14:1–16.

74. Luttik AK, Tejwani L, Ju H, Driessen T, Smeets C. Differential effects of Wnt- β -catenin signaling in Purkinje cells and Bergmann glia in SCA1. BioRxiv. 2021;1–26.

75. Selimi F, Lohof AM, Heitz S, Lalouette A, Jarvis CI, Bailly Y, et al. Lurcher GRID2-induced death and depolarization can Be dissociated in cerebellar Purkinje cells. Neuron. 2003;37:813–9.

76. Utine GE, Halilo□lu G, Salanci B, Çetinkaya A, Kiper PÖ, Alanay Y, et al. A homozygous deletion in GRID2 causes a human phenotype with cerebellar ataxia and atrophy. J. Child Neurol. 2013;28:926–32.

77. Hills LB, Masri A, Konno K, Kakegawa W, Lam ATN, Lim-Melia E, et al. Deletions in GRID2 lead to a recessive syndrome of cerebellar ataxia and tonic upgaze in humans. Neurology. 2013;81:1378–86.

78. Djukic B, Kristen B. Casper, Benjamin D. Philpot, Lih-Shen Chin and KDM. Conditional Knock-Out of Kir4.1 Leads to Glial Membrane Depolarization, Inhibition of Potassium and Glutamate Uptake,

and Enhanced Short-Term Synaptic Potentiation. J. Neurosci. 2007;27:11354–65.

79. Rothstein J, Dykes-Hoberg M, Pardo C, Bristol L, Jin L, Kuncl R, et al. Antisense knockout of glutamate transporters reveals a predominant role for astroglial glutamate transport in excitotoxicity and clearance of extracellular glutamate. Neuron [Internet]. 1996;16:675–86. Available from: papers2://publication/uuid/327F682D-2D03-48C7-A0E6-A57E2CD92157

80. Farmer WT, Chierzi S, Lui C, Zaelzer C, Jones E V, Bally BP, et al. Neurons diversify astrocytes in the adult brain through sonic hedgehog signaling. Science (80-.). 2016;351:849.

81. Burright EN, Clark BH, Servadio A, Matilla T, Feddersen RM, Yunis WS, et al. SCA1 transgenic mice: A model for neurodegeneration caused by an expanded CAG trinucleotide repeat. Cell. 1995;82:937–48.

82. Chopra R, Bushart DD, Cooper JP, Yellajoshyula D, Morrison LM, Huang H, et al. Altered Capicua expression drives regional Purkinje neuron vulnerability through ion channel gene dysregulation in spinocerebellar ataxia type 1. Hum Mol Genet. 2020;29:3249–65.

83. White JJ, Bosman LWJ, Blot FGC, Osório C, Kuppens BW, Krijnen WHJJ, et al. Region-specific preservation of Purkinje cell morphology and motor behavior in the ATXN1[82Q] mouse model of spinocerebellar ataxia 1. Brain Pathol. 2021;31:1–17.

	Posterior vs Anterior Vermis	
	Fold Change	FDR
Kcng4	-1.66	5.61E-09
Aldoc	1.65	3.96E-05

CCAV		CCPV		CHH	
logFC	**Gene**	**logFC**	**Gene**	**logFC**	**Gene**
14.09	Ddx3y	12.27	Uty	13.47	Eif2s3y
13.58	Eif2s3y	11.87	Eif2s3y	13.07	Kdm5d
13	Kdm5d	11.35	Kdm5d	12.34	Ddx3y
12.06	Uty	10.69	Ddx3y	12.32	Uty
-0.36	Sipa1l1	0.5	Rik	4.92	A230087F16Rik
-0.37	Chst11	-0.48	Ddx3x	4.75	Lamp5
-0.43	Jmjd4	-0.55	Kdm6a	0.53	1700017B05Rik
-0.45	Ddx3x	-0.61	Kdm5c	-0.42	Ddx3x
-0.52	Kdm6a	-0.69	Eif2s3x	-0.52	5530601H04Rik
-0.61	Kdm5c	-15.17	Xist	-0.55	Eif2s3x
-0.72	Eif2s3x			-0.56	Kdm5c
-1.18	Slc2a13			-0.63	Kdm6a
-14.47	Xist			-14.2	Xist

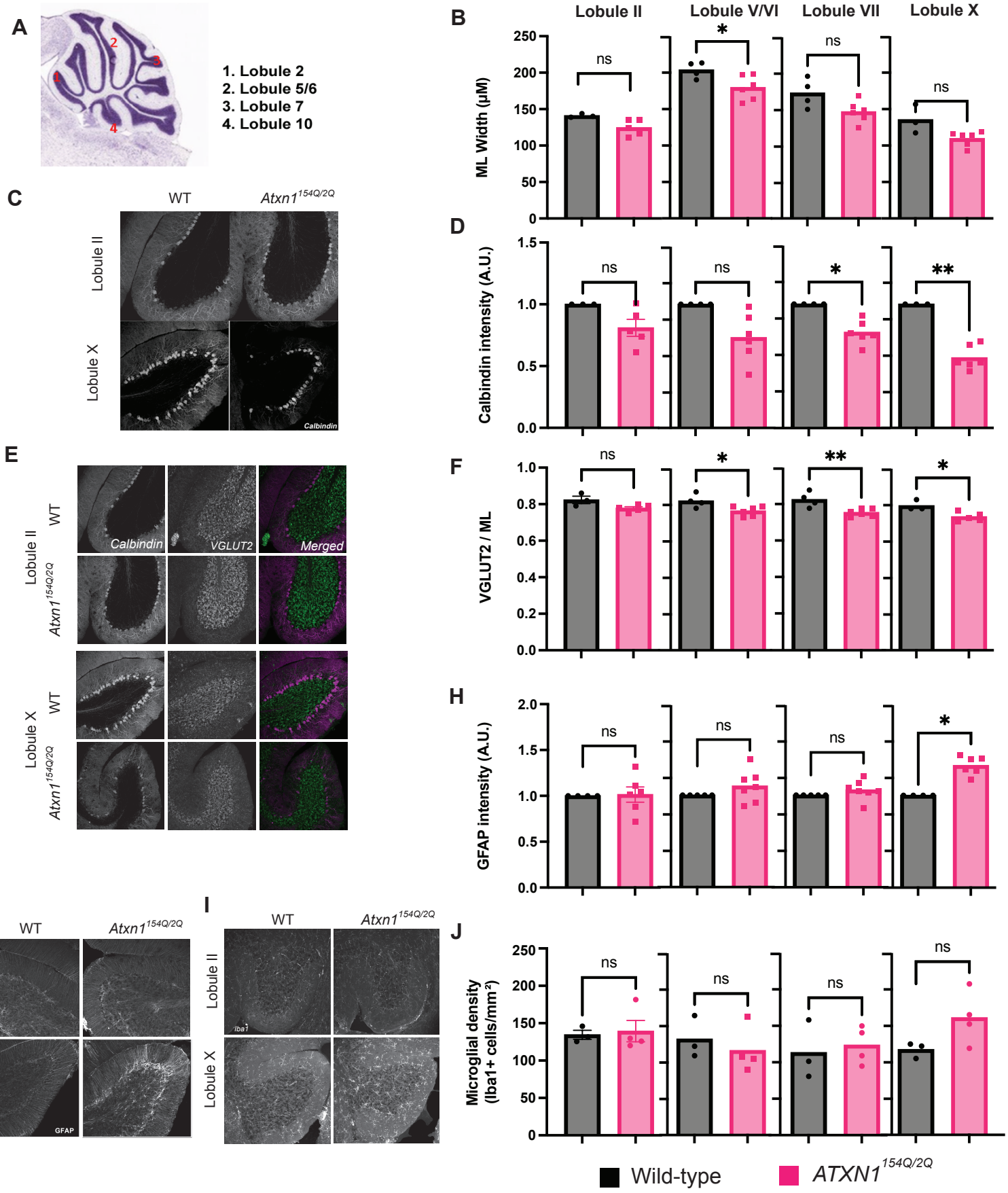
A
1. Lobule 2
2. Lobule 5/6
3. Lobule 7
4. Lobule 10
B
Lobule II
Lobule V/VI
Lobule VII
Lobule X
ML Width (µM)
C
WT
Atxn1 154Q/2Q
Lobule II
Lobule X
Calbindin
D
Calbindin intensity (A.U.)
E
Lobule II
Lobule X
WT
Atxn1 154Q/2Q
Calbindin
VGLUT2
Merged
F
VGLUT2 / ML
H
GFAP intensity (A.U.)
G
GFAP
I
Iba1
J
Microglial density (Iba1+ cells/mm²)
ns
Wild-type
ATXN1 154Q/2Q

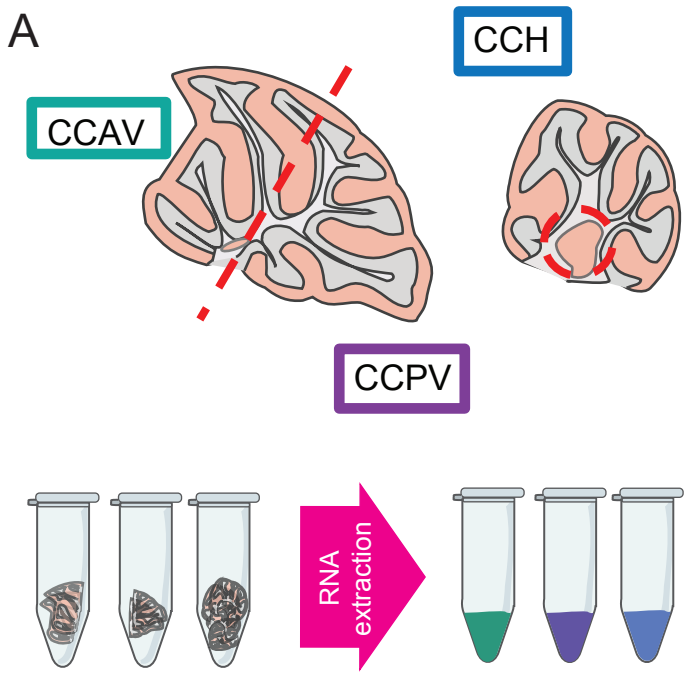
A
CCAV
CCH
CCPV
RNA extraction

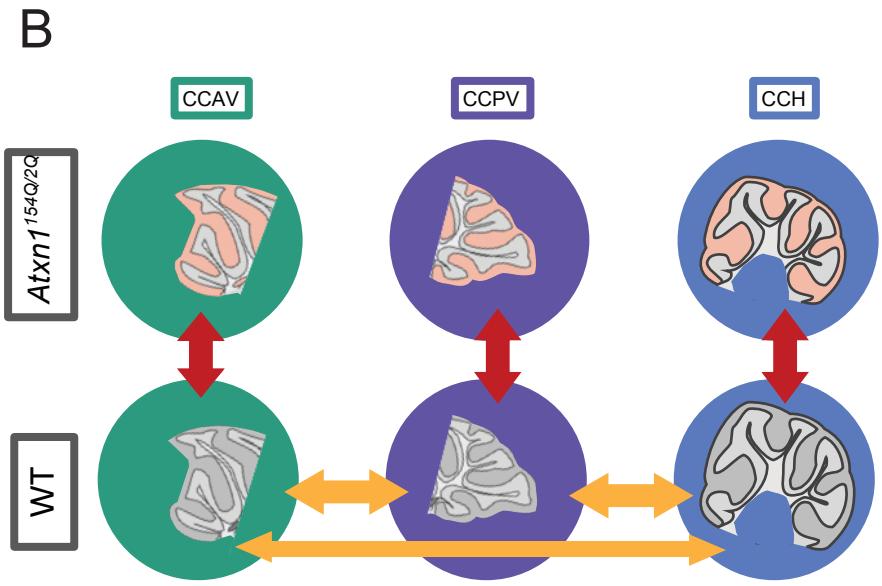
B
CCAV
CCPV
CCH
Atxn1154Q/2Q
WT

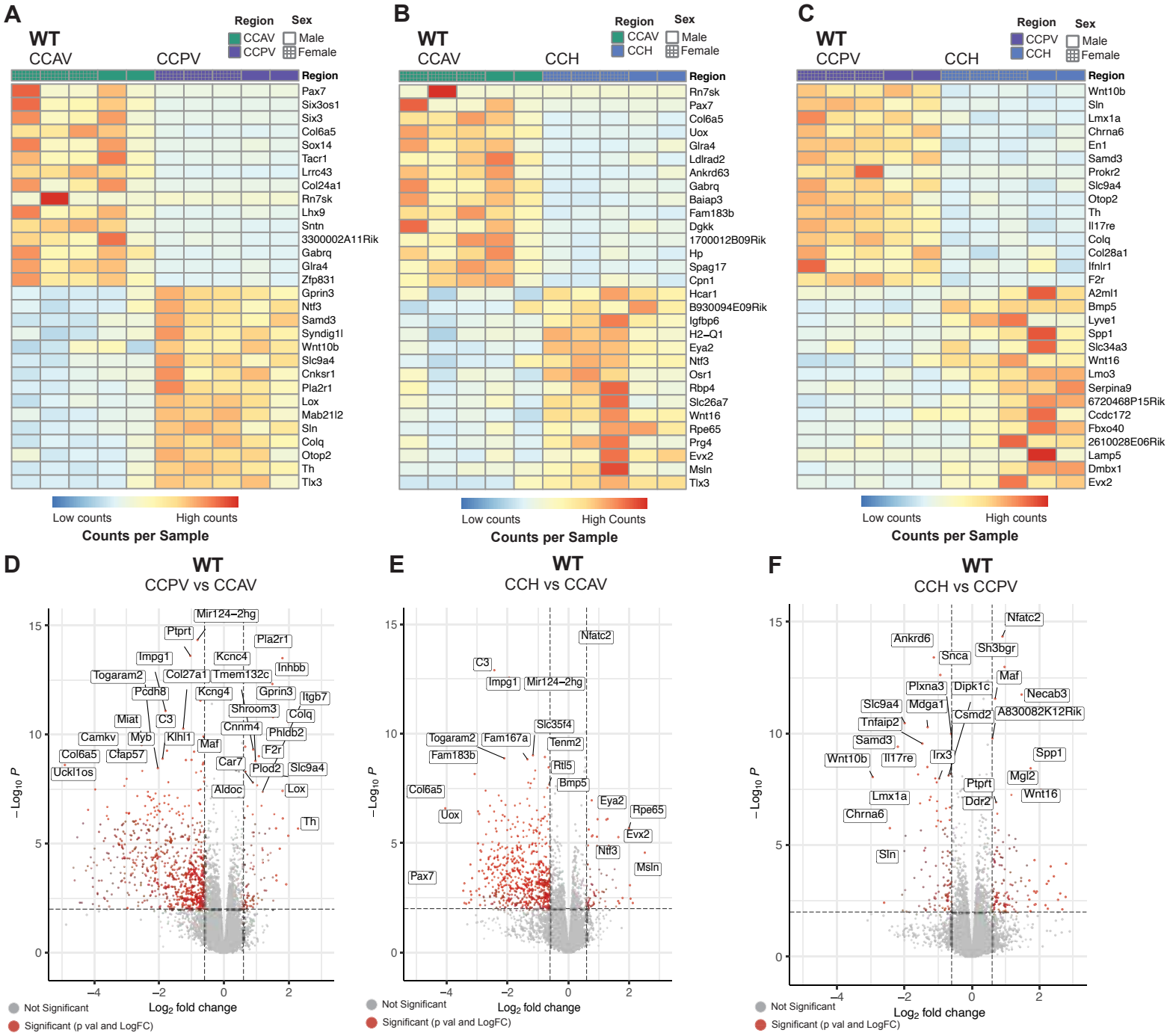
A
WT
CCAV
CCPV
Region
Sex
CCAV
CCPV
Male
Female
Pax7
Six3os1
Six3
Col6a5
Sox14
Tacr1
Lrrc43
Col24a1
Rn7sk
Lhx9
Sntn
3300002A11Rik
Gabrq
Glra4
Zfp831
Gprin3
Ntf3
Samd3
Syndig1l
Wnt10b
Slc9a4
Cnksr1
Pla2r1
Lox
Mab21l2
Sln
Colq
Otop2
Th
Tlx3
Low counts
High counts
Counts per Sample
B
WT
CCAV
CCH
Region
Sex
CCAV
CCH
Male
Female
Rn7sk
Pax7
Col6a5
Uox
Glra4
Ldlrad2
Ankrd63
Gabrq
Baiap3
Fam183b
Dgkk
1700012B09Rik
Hp
Spag17
Cpn1
Hcar1
B930094E09Rik
Igfbp6
H2–Q1
Eya2
Ntf3
Osr1
Rbp4
Slc26a7
Wnt16
Rpe65
Prg4
Evx2
Msln
Tlx3
Low counts
High Counts
Counts per Sample
C
WT
CCPV
CCH
Region
Sex
CCPV
CCH
Male
Female
Wnt10b
Sln
Lmx1a
Chrna6
En1
Samd3
Prokr2
Slc9a4
Otop2
Th
Il17re
Colq
Col28a1
Ifnlr1
F2r
A2ml1
Bmp5
Lyve1
Spp1
Slc34a3
Wnt16
Lmo3
Serpina9
6720468P15Rik
Ccdc172
Fbxo40
2610028E06Rik
Lamp5
Dmbx1
Evx2
Low counts
High counts
Counts per Sample
D
WT
CCPV vs CCAV
Mir124–2hg
Ptprt
Pla2r1
Impg1
Kcnc4
Inhbb
Togaram2
Col27a1
Tmem132c
Pcdh8
Kcng4
Gprin3
Itgb7
Shroom3
Colq
Miat
C3
Cnnm4
Phldb2
Camkv
Myb
Klhl1
Maf
F2r
Col6a5
Ctap57
Car7
Plod2
Slc9a4
Uckl1os
Aldoc
Lox
Th
Not Significant
Significant (p val and LogFC)
Log2 fold change
E
WT
CCH vs CCAV
Nfatc2
C3
Impg1
Mir124–2hg
Slc35f4
Togaram2
Fam167a
Tenm2
Fam183b
Rtl5
Bmp5
Col6a5
Eya2
Rpe65
Uox
Evx2
Ntf3
Msln
Pax7
Not Significant
Significant (p val and LogFC)
Log2 fold change
F
WT
CCH vs CCPV
Nfatc2
Ankrd6
Sh3bgr
Snca
Maf
Plxna3
Dipk1c
Necab3
Slc9a4
Mdga1
Csmd2
A830082K12Rik
Tnfaip2
Samd3
Spp1
Wnt10b
Il17re
Irx3
Mgl2
Ptprt
Lmx1a
Ddr2
Wnt16
Chrna6
Sln
Not Significant
Significant (p val and LogFC)
Log2 fold change
G
KEGG Pathway analysis
Neuroactive ligand–receptor interaction
Protein digestion and absorption
Calcium signaling pathway
cAMP signaling pathway
Taste transduction
Gastric acid secretion
Nicotine addiction
Insulin secretion
Pathways of neurodegeneration – multiple diseases
Hippo signaling pathway
Huntington disease
Sulfur metabolism
Melanogenesis
Focal adhesion
Human papillomavirus infection
Signaling pathways regulating pluripotency of stem cells
AvP (159)
AvH (139)
PvH (135)
GeneRatio
0.05
0.10
0.15
0.20
p.adjust
0.01
0.02
0.03
0.04

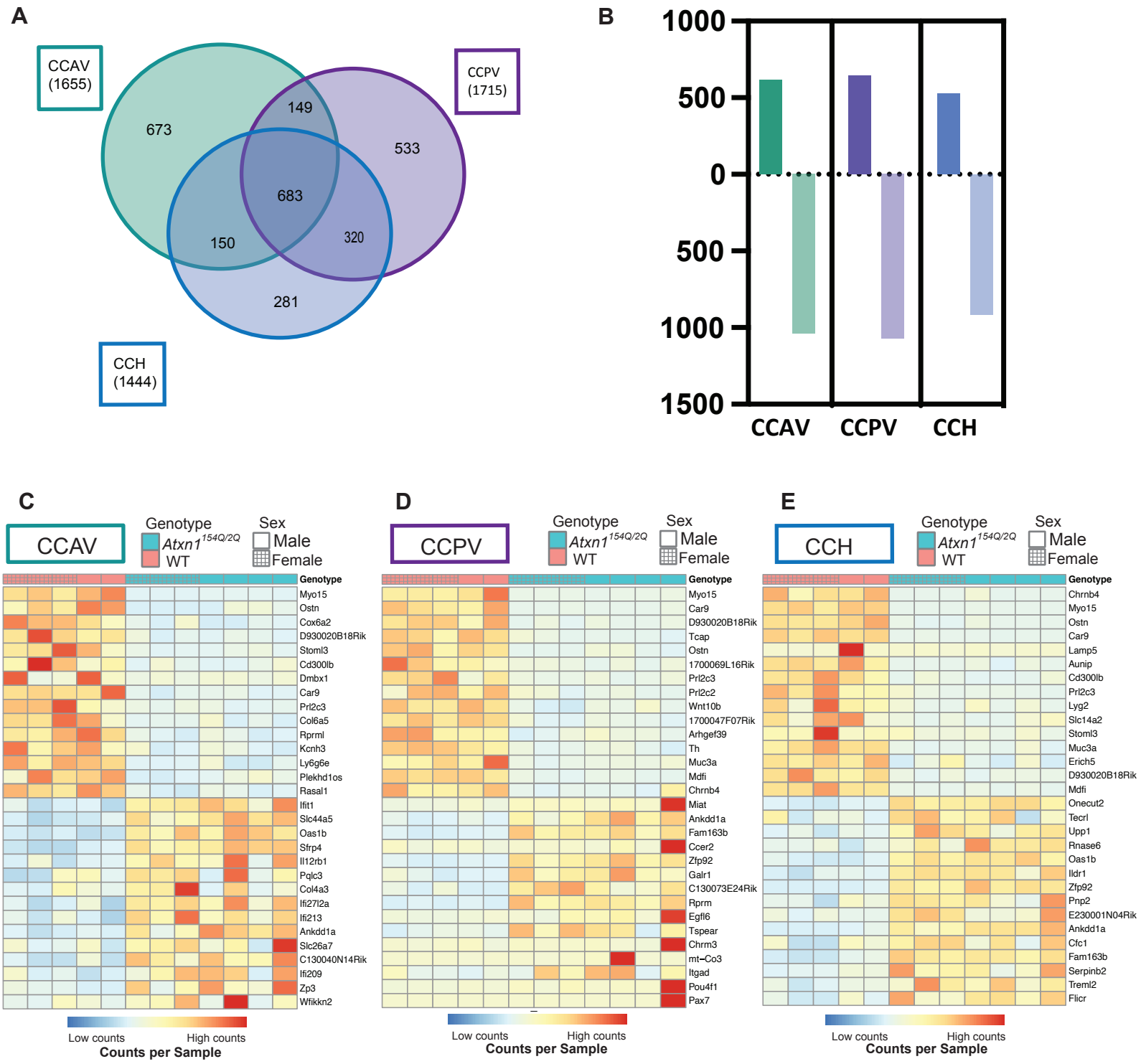
A
CCAV (1655)
CCPV (1715)
CCH (1444)
673
149
533
683
150
320
281
B
1000
500
0
500
1000
1500
CCAV
CCPV
CCH
C
CCAV
Genotype
Atxn1 154Q/2Q
WT
Sex
Male
Female
Genotype
Myo15
Ostn
Cox6a2
D930020B18Rik
Stoml3
Cd300lb
Dmbx1
Car9
Prl2c3
Col6a5
Rprml
Kcnh3
Ly6g6e
Plekhd1os
Rasal1
Ifit1
Slc44a5
Oas1b
Sfrp4
Il12rb1
Pqlc3
Col4a3
Ifi27l2a
Ifi213
Ankdd1a
Slc26a7
C130040N14Rik
Ifi209
Zp3
Wfikkn2
Low counts
High counts
Counts per Sample
D
CCPV
Genotype
Atxn1 154Q/2Q
WT
Sex
Male
Female
Genotype
Myo15
Car9
D930020B18Rik
Tcap
Ostn
1700069L16Rik
Prl2c3
Prl2c2
Wnt10b
1700047F07Rik
Arhgef39
Th
Muc3a
Mdfi
Chrnb4
Miat
Ankdd1a
Fam163b
Ccer2
Zfp92
Galr1
C130073E24Rik
Rprm
Egfl6
Tspear
Chrm3
mt-Co3
Itgad
Pou4f1
Pax7
Low counts
High counts
Counts per Sample
E
CCH
Genotype
Atxn1 154Q/2Q
WT
Sex
Male
Female
Genotype
Chrnb4
Myo15
Ostn
Car9
Lamp5
Aunip
Cd300lb
Prl2c3
Lyg2
Slc14a2
Stoml3
Muc3a
Erich5
D930020B18Rik
Mdfi
Onecut2
Tecrl
Upp1
Rnase6
Oas1b
Ildr1
Zfp92
Pnp2
E230001N04Rik
Ankdd1a
Cfc1
Fam163b
Serpinb2
Treml2
Flicr
Low counts
High counts
Counts per Sample

KEGG
Malaria
Glutamatergic synapse
Aldosterone synthesis and secretion
Insulin secretion
GnRH secretion
Gastric acid secretion
Cholinergic synapse
Oxytocin signaling pathway
Calcium signaling pathway
AGE−RAGE signaling pathway in diabetic complications
Pancreatic secretion
Nitrogen metabolism
Dilated cardiomyopathy
Cushing syndrome
African trypanosomiasis
Chronic myeloid leukemia
PPAR signaling pathway
GABAergic synapse
Growth hormone synthesis, secretion and action
Arrhythmogenic right ventricular cardiomyopathy
Morphine addiction
Hypertrophic cardiomyopathy
Apoptosis
Protein digestion and absorption
cAMP signaling pathway
MAPK signaling pathway
Dopaminergic synapse
Circadian entrainment
Spinocerebellar ataxia
Long−term depression
Estrogen signaling pathway
Hepatitis B
Amphetamine addiction
Hepatitis C
Phosphatidylinositol signaling system
ErbB signaling pathway
Inositol phosphate metabolism
Focal adhesion
Nicotine addiction
Measles
Retrograde endocannabinoid signaling
PI3K−Akt signaling pathway
Fc gamma R−mediated phagocytosis
Thyroid hormone signaling pathway
Gastric cancer
Wnt signaling pathway
Regulation of actin cytoskeleton
Neuroactive ligand−receptor interaction
Cocaine addiction
Colorectal cancer
Inflammatory bowel disease
Pancreatic cancer
Small cell lung cancer
CCAV (411)
CCPV (389)
CCH (391)
GeneRatio
0.02
0.04
0.06
p.adjust
0.01
0.02
0.03
0.04

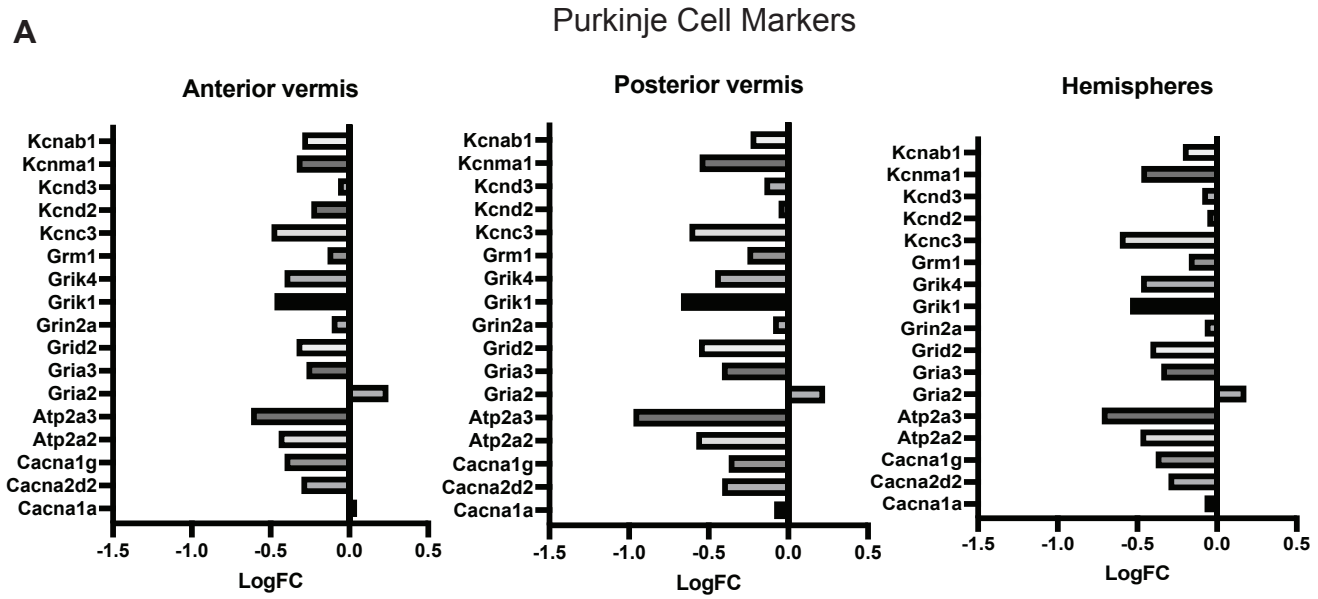
A
Purkinje Cell Markers
Anterior vermis
Posterior vermis
Hemispheres
Kcnab1
Kcnma1
Kcnd3
Kcnd2
Kcnc3
Grm1
Grik4
Grik1
Grin2a
Grid2
Gria3
Gria2
Atp2a3
Atp2a2
Cacna1g
Cacna2d2
Cacna1a
-1.5
-1.0
-0.5
0.0
0.5
LogFC

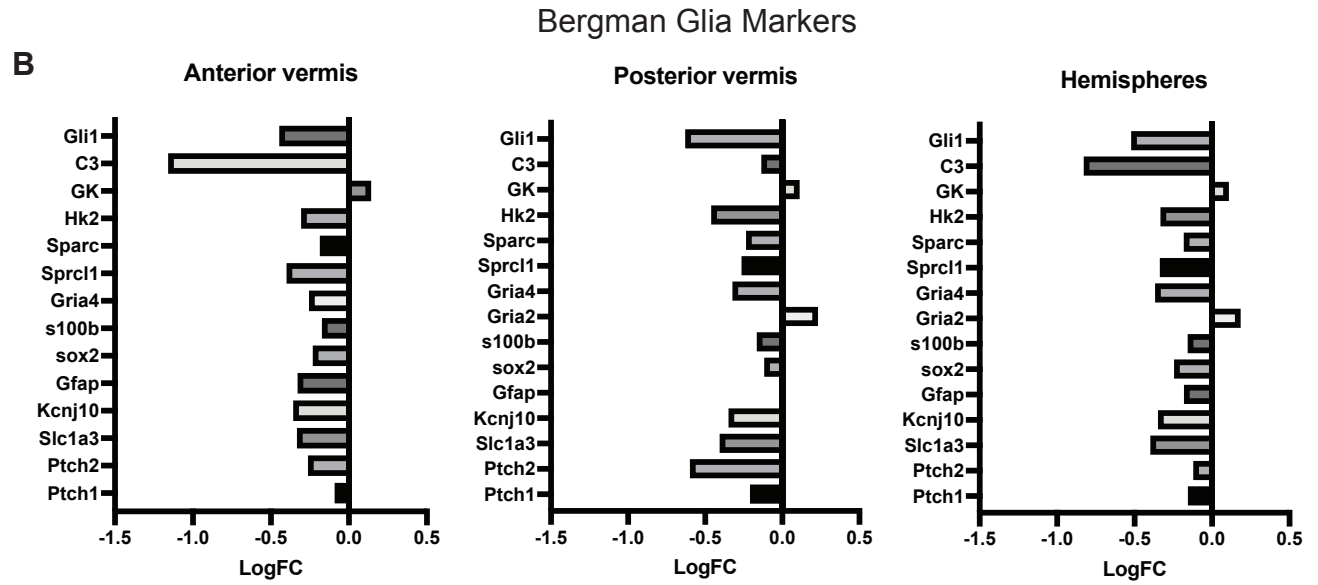
B
Bergman Glia Markers
Anterior vermis
Posterior vermis
Hemispheres
Gli1
C3
GK
Hk2
Sparc
Sprcl1
Gria4
Gria2
s100b
sox2
Gfap
Kcnj10
Slc1a3
Ptch2
Ptch1
-1.5
-1.0
-0.5
0.0
0.5
LogFC

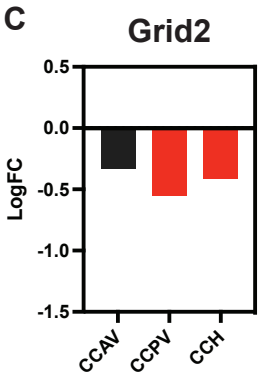
C
Grid2
LogFC
0.5
0.0
-0.5
-1.0
-1.5
CCAV
CCPV
CCH

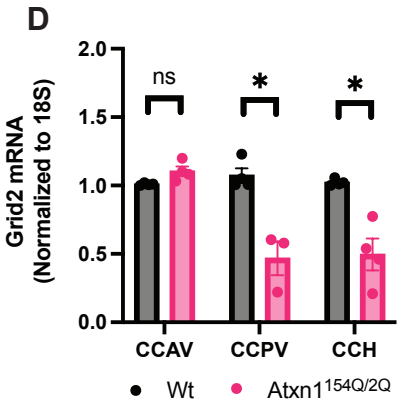
D
Grid2 mRNA
(Normalized to 18S)
2.0
1.5
1.0
0.5
0.0
ns
*
*
CCAV
CCPV
CCH
Wt
Atxn1154Q/2Q

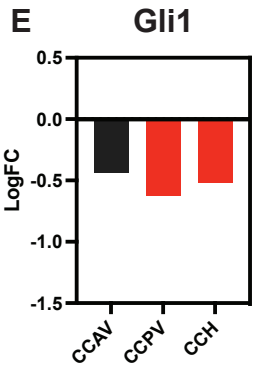
E
Gli1
LogFC
0.5
0.0
-0.5
-1.0
-1.5
CCAV
CCPV
CCH

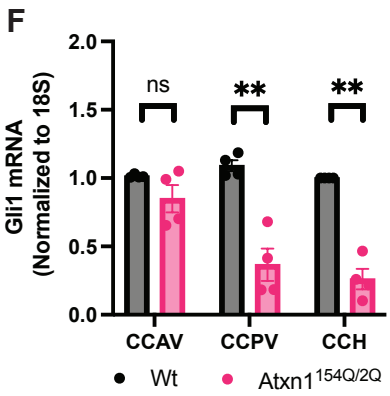
F
Gli1 mRNA
(Normalized to 18S)
2.0
1.5
1.0
0.5
0.0
ns
**
**
CCAV
CCPV
CCH
Wt
Atxn1154Q/2Q